ACS OMEGA

http://pubs.acs.org/journal/acsodf

Article

Photoinduced Photosensitizer–Antibody Conjugates Kill HIV Env-Expressing Cells, Also Inactivating HIV

Mohammad Sadraeian, Edgar Ferreira da Cruz, Ross W. Boyle, Calise Bahou, Vijay Chudasama, Luiz Mário Ramos Janini, Ricardo Sobhie Diaz,* and Francisco E. G. Guimarães

Cite This: https://doi.org/10.1021/acsomega.1c01721

Read Online

ACCESS | Metrics & More | Article Recommendations | Supporting Information

ABSTRACT: HIV-infected cells persist for decades in patients administered with antiretroviral therapy (ART). Meanwhile, an alarming surge in drug-resistant HIV viruses has been occurring. Addressing these issues, we propose the application of photoimmunotherapy (PIT) against not only HIV Env-expressing cells but also HIV. Previously, we showed that a human anti-gp41 antibody (7B2) conjugated to cationic or anionic photosensitizers (PSs) could specifically target and kill the HIV Env-expressing cells. Here, our photolysis studies revealed that the binding of photoimmunoconjugates (PICs) on the membrane of HIV Env-expressing cells is sufficient to induce necrotic cell death due to physical damage to the membrane by singlet oxygen, which is independent of the type of PSs. This finding persuaded us to study the virus photoinactivation of PICs using two HIV-1 strains, X4 HIV-1 NL4-3 and JR-CSF virus. We observed that the PICs could destroy the viral strains, probably via physical damage on the HIV envelope. In conclusion, we report the application of PIT as a possible dual-tool for HIV immunotherapy and ART by killing HIV-expressing cells and cell-free HIV, respectively.

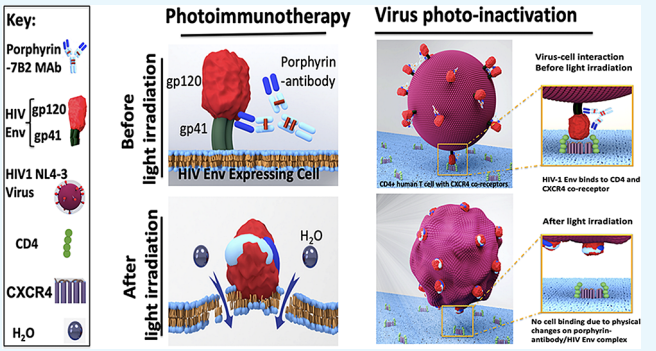

1. INTRODUCTION

HIV-infected cells persist in patients on antiretroviral therapy (ART), and viremia returns if ART is halted.[1,2] Furthermore, recent surveys by the World Health Organization (WHO) have uncovered an alarming surge in resistance to crucial HIV antiretrovirals.[3] Currently, ART aims to maintain viral loads below detection limits (BDLs) of current commercial assays by blocking viral replication and preventing the spread or growth of viral reservoirs for preserving CD4+ T-cells, but its use is restricted by long-term end-organ drug toxicities and the expansion of viral resistance.[4] In addition, persistent low-level viremia can remain even when under ART, potentially from tissues with low drug penetration or residual virus replication in latently infected cells.[5−7] Additionally, the clonal expansion of HIV-infected cells may contribute to the size of the HIV reservoir.[8] Furthermore, defective HIV-1 proviruses, which prevail after long-term "suppressive" ART[9] (although not able to produce a full replicative cycle), will produce HIV m-RNA and HIV proteins, which will contribute to the deleterious HIV-related microinflammation, despite years of plasma HIV-RNA levels BDL during ART.[10] In fact, antiproliferative drugs that will reduce the size of HIV reservoir in lymphocytes among individuals under long-term "suppressive" ART will decrease total HIV DNA and decrease the cell activation markers in CD4+ T cells.[11] Thus, this demands the design of therapeutic ART alternatives and novel strategies for directly killing the latently infected cells or cells harboring defective provirus, which may address limitations of ART and immunotherapy (IT), ultimately acquiring the HIV remission without the use of antiretrovirals.

Several types of immunotherapeutic strategies, with limited success, have been studied to specifically kill HIV-infected cells using HIV Env-targeting antibodies.[12] Most of these results were dependent on the preexisting resistance of circulating/reservoir strains, and in all cases, viremia rapidly rebounded upon MAb decay or cessation.[13] Thus, strategies to fight both preexisting and de novo development of viral resistance remain a target of antibody-based therapy for chronic infection.

In acute infection, conjugation of antibodies with more toxic drugs, including chemical drugs such as doxorubicin[14] or immunogenic toxins such as ricin,[15,16] pulchellin,[17] and shiga toxin,[18] may be tolerable as a short-term solution to ensure rapid and complete cytotoxicity to treat the acute infection.[19] In contrast, to treat chronic infections such as HIV infection, antibody-based immunotherapies that are more amenable to

Received: March 30, 2021
Accepted: May 27, 2021

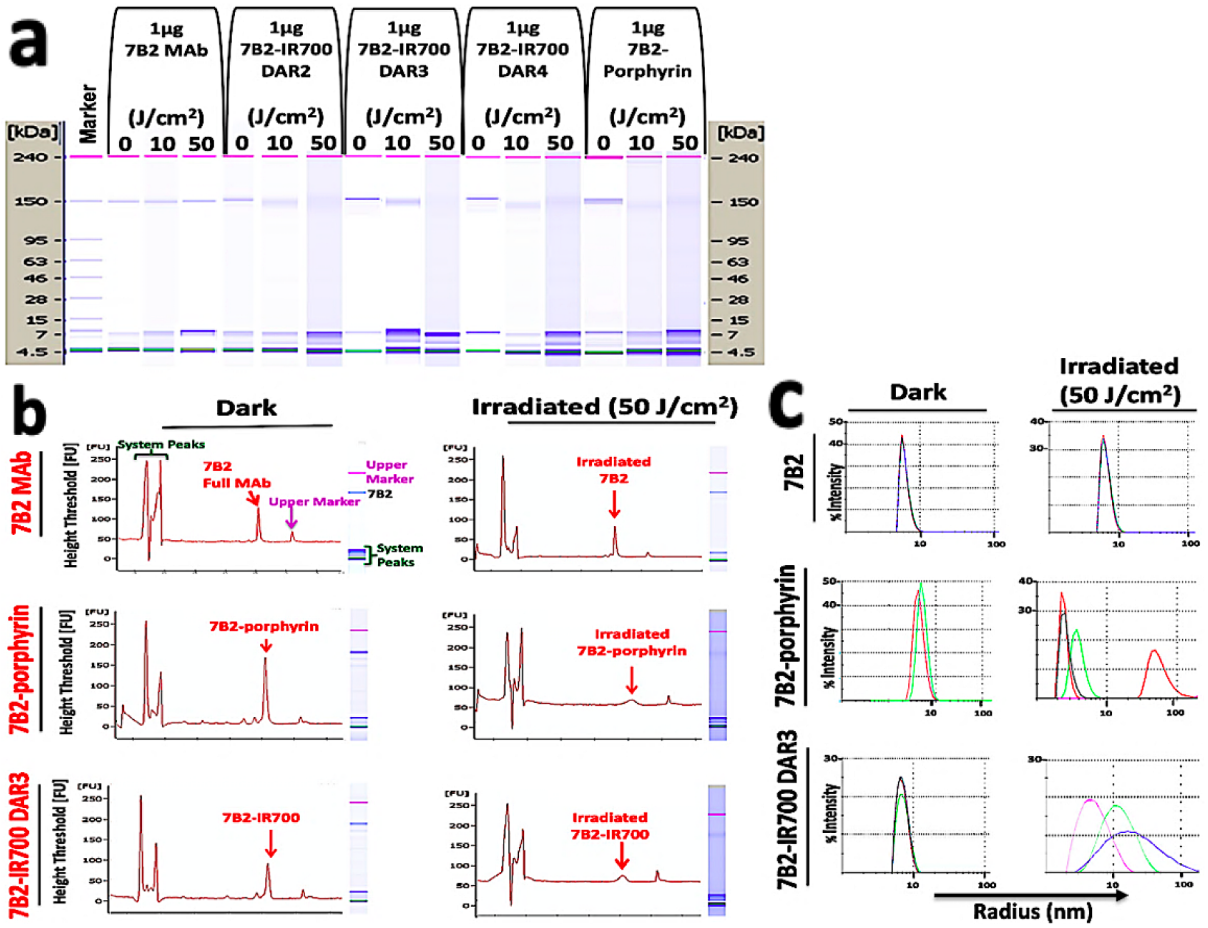

Figure 1. Study of the effect of irradiation on the structure of PICs. (a and b) Microcapillary electrophoresis (a) and electropherogram (b) of 7B2 MAb and PICs of nonreduced 7B2 MAb, 7B2-porphyrin, and 7B2-IR700 with different DARs of 2, 3, and 4, before and after irradiation with 10 or 50 J/cm^2. (a) In a dose-dependent manner, protein bands of PICs disappeared with forming smear, while the bands of naked 7B2 antibody were preserved. Size standards are indicated on the side of each "gel." (b) The system peaks and upper marker in the electropherogram are indicated in green and violet, respectively. (c) Histograms of PICs, before and after irradiation, monitor how the hydrodynamic radius (R_h), shape, and solubility of PICs significantly changed after irradiation with power density of 50 J/cm^2, while naked 7B2 antibody showed preservation. The irradiated 7B2-IR700 showed different types of aggregation in comparison to the irradiated 7B2-porphyrin. Each curve in an individual color represents the average of 10 acquisitions.

long-term use with more long-lasting effects may provide an optimal candidate.

Recently, we introduced HIV photoimmunotherapy (HIV PIT), which is an emerging anti-HIV IT via arming HIV MAbs with photosensitizers (PSs) targeting HIV Env-expressing cells.[20] PIT is the targeted form of conventional photodynamic therapy (PDT), achieved through the conjugation of PS with MAbs targeting specific cell surface receptors.[21,22] A non-ionizing light of a particular wavelength can activate PSs to kill the cells by generating reactive oxygen species (ROS), including hydrogen peroxide, hydroxyl radicals, superoxide, and singlet oxygen.[20,21] PIT has certain advantages over immunotoxins (ITs) or radioimmunotherapy (RIT) to eradicate infected cells.[23] In PIT, target selection is determined not only by antibodies but also by light, regarding the time and local irradiation. Moreover, PIT is a minimally invasive, safer, and cheaper therapy than ITs or RIT,[21] making PIT an appropriate candidate to treat chronic infections such as HIV. Our recent findings on PIT might help to add more advantages to this list.

In previous studies, we produced two different photoimmunoconjugates (PICs) via conjugation of a human anti-gp41 antibody (7B2)[24] with two PSs, cationic porphyrin and anionic IR700. We employed two different strategies for conjugation to the antibody: lysine conjugation using a phthalocyanine IRDye700DX dye[25] and "Click" conjugation using an azide-bearing porphyrin with a strained alkyne attached via a disulfide bridge linker.[26] MAb 7B2 is a non-neutralizing antibody that recognizes both virus particles and HIV Env-expressing cells.[27] We demonstrated that the targeted phototoxicity is independent of the PS payload.

In this study, the comparison between PICs is of interest concerning the physical and immunological changes in PICs during irradiation and the mechanism of in vitro cytotoxicity. Targeted phototoxicity seems to be independent of cell internalization while being dependent on singlet oxygen generation by PSs, which physically damages both the antibody and the cell membrane. This finding persuaded us to study the virus photoinactivation of PICs using HIV-1 strains. Unlike other HIV immunoconjugates, we observed that the PICs kill the HIV Env-expressing cells and destroy the virus and so can be considered a tool for ART.

https://doi.org/10.1021/acsomega.1c01721
ACS Omega XXXX, XXX, XXX−XXX

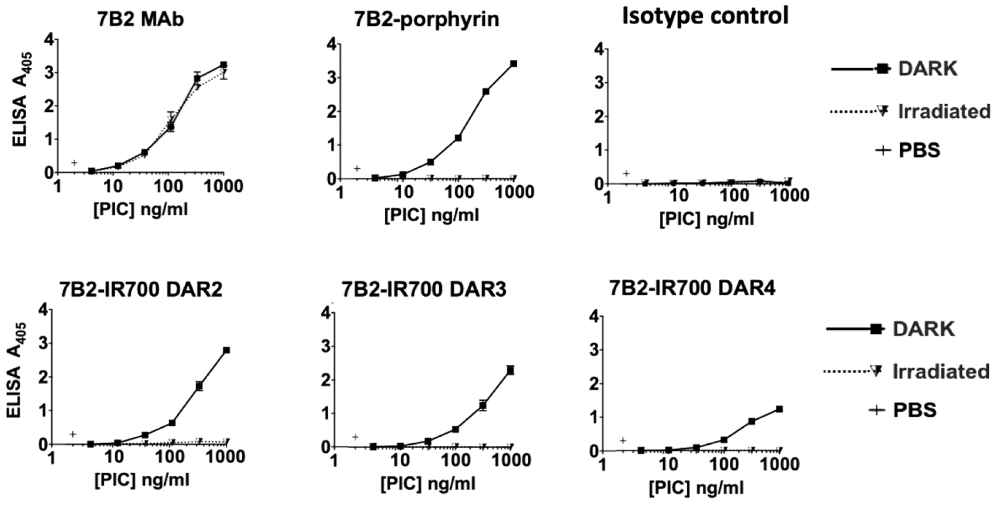

Figure 2. Study of the effect of irradiation on the binding ability of PICs. ELISA plates were coated with gp41 antigen, as a peptide representing 7B2's epitope. PICs were kept in the dark or irradiated with 50 J/cm^2, before incubation with gp41. The irradiation of PICs resulted in complete loss of binding ability, while naked 7B2 antibody retained the binding ability. Mouse IgG1 Ab was used as an isotype control. Data are mean ± SEM (n = 2) with two individual experiments.

2. RESULTS AND DISCUSSION

2.1. Study the Effect of Irradiation on the Structure and Binding Ability of PICs. Previously, two generations of PICs were produced: homogeneous porphyrin-7B2 with a constant drug−antibody ratio (DAR) of 4 and heterogeneous IR700-PICs with different DARs of 2, 3, and 4.[19] Herein, the effects of light irradiation on the PICs were studied, physically and immunologically, using microcapillary electrophoresis, dynamic light scattering (DLS), and ELISA. Both porphyrin-7B2 and IR700-7B2 were irradiated equally by a custom-made LED device with a broad spectrum of light (380−780 nm).[19]

Results of microcapillary electrophoresis of nonreduced antibody (H and L chains) and PICs, before and after irradiation, revealed that the protein bands of 7B2-PICs disappeared in a dose-dependent manner with a power density of 10 and 50 J/cm^2. The irradiation with 10 J/cm^2 affected the molecular sizes of 7B2-IR700 with different DARs and at a higher dose of 50 J/cm^2 showed smear formation, probably due to the release of the hydrophobic ligand of IR700. A similar smear of bands was observed for 7B2-porphyrin (Figure 1a). Electropherogram of irradiated PICs demonstrated decreasing bands related to the full-length MAbs; however, no truncated protein band was observed. In contrast, the naked 7B2 antibody bands did not change during irradiation (Figure 1b).

DLS measurements demonstrated that the irradiation of PICs with 50 J/cm^2 yielded different types of aggregation, with significant changes with regard to the molecule's average size (hydrodynamic radius, R_h), shape, and solubility, while 7B2 showed preservation. Interestingly, the irradiated 7B2-IR700 showed different types of aggregation in comparison to the irradiated 7B2-porphyrin (Figure 1c). Indirect ELISA showed that the 7B2-based PICs lost their binding ability to the gp41 after irradiation with 50 J/cm^2, while the irradiated 7B2 MAb showed preserved binding ability (Figure 2). The results signify that the excited PSs may destroy the structure of the antibodies and the binding ability of PICs.

2.2. Singlet Oxygen Generation. We studied photobleaching of ABDA by singlet oxygen ($^1O_2$) generated during irradiation of PSs and PICs in the media with no applying cells, as a function of continuous 380−780 nm irradiation times at a power density of 30 mW/cm^2 in water solution. ABDA rapidly and quantitatively reacts with $^1O_2$, resulting in the loss of absorbance intensity of ABDA at 400 nm.

First, singlet oxygen generation by porphyrin azide was compared before and after conjugation, with a 4× serial concentration of porphyrin azide (156, 625, and 2500 nM) and 625 nM 7B2-porphyrin DAR4 (containing 2500 nM porphyrin in the interaction with 625 nM antibody). The changes in ABDA absorption at 400 nm were measured as a function of irradiation time (0−50 min) on the generation of singlet oxygen by porphyrin azide in comparison to porphyrin−antibody. The results show that porphyrin's ability to produce singlet oxygen has decreased after conjugation due to lower availability of oxygen in the media[28] (Figure 3a).

Afterward, singlet oxygen generation by porphyrin-7B2 and IR700-PICs was compared using an irradiation time of 50 min. Porphyrin-7B2 (DAR of 4) showed more singlet oxygen generation than IR700-7B2 (DAR of 2) but less than IR700-PICs (DARs of 3 and 4). In the presence of 0.01% sodium azide, the generated singlet oxygen was quenched. The controls were without PIC or with naked 7B2 antibody (controls) (Figure 3b). UV−vis absorbance spectra demonstrated photobleaching of ABDA upon 40 min irradiation in the presence of PICs. Interestingly, the absorption band of porphyrin was quenched during irradiation due to the photodegradation. In contrast, the absorption band of IR700 was preserved (Figure 3c). The controls include 7B2 and double-distilled (DD) water (n = 3).

2.3. Phototoxicity Based on the PIC Localization Using FACS and Two-Photon Microscopy. We studied the singlet oxygen-induced phototoxicity based on the PIC localization to investigate whether the singlet oxygen and physical changes in the antibody on the membrane are responsible for the cytotoxicity induced by PIT. Three models of PIC localization included the internalized PICs and two membrane-binding models irradiated in the presence and absence of sodium azide as a $^1O_2$ quencher (Figures 4 and S1). A parallel study was performed on control 293T cells (Figure S2). The hypothesis is that the azide not only prevents

https://doi.org/10.1021/acsomega.1c01721
ACS Omega XXXX, XXX, XXX−XXX

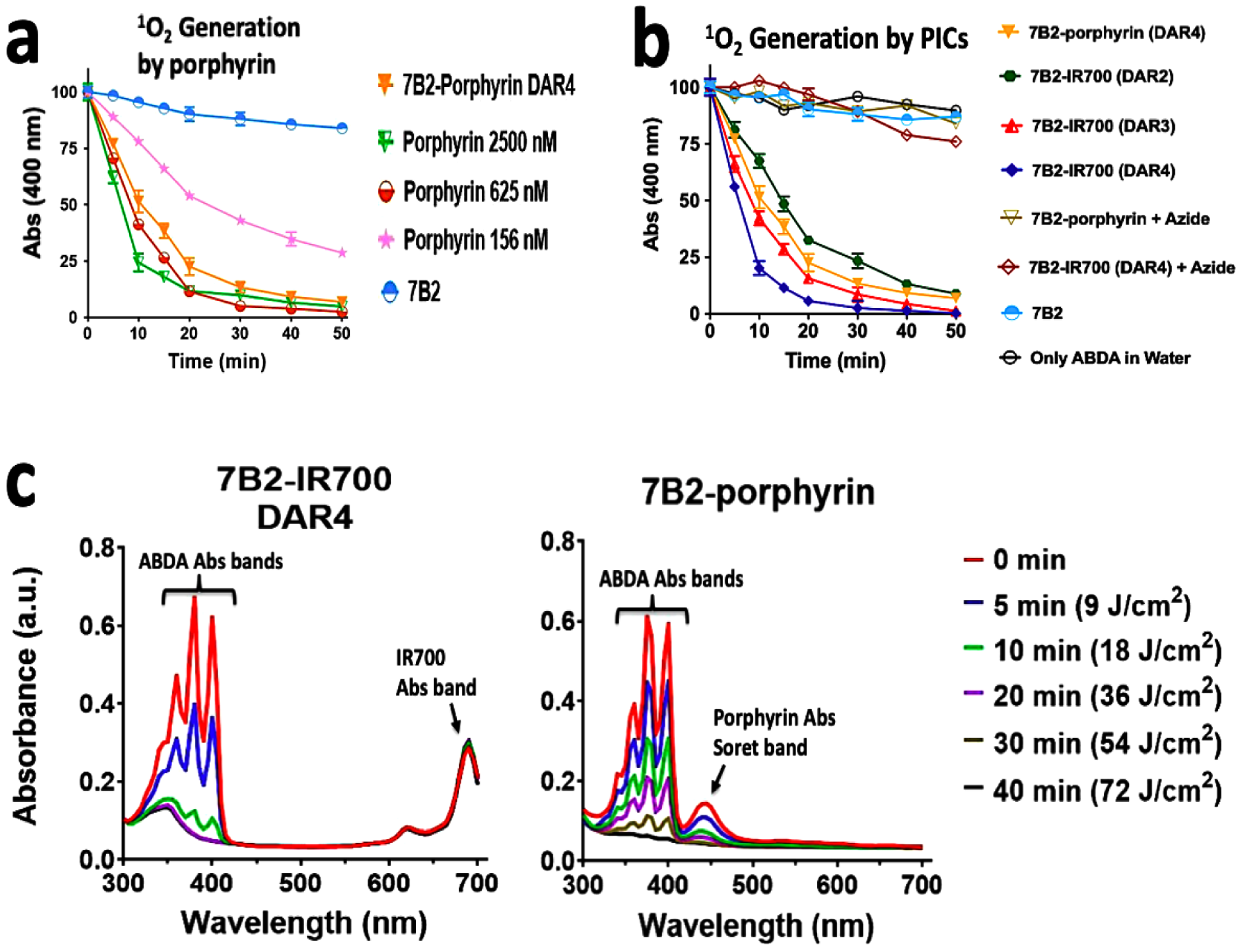

Figure 3. Study of singlet oxygen generation by PSs and PICs, in media with no applying cells, as a function of continuous 380−780 nm irradiation times. (a) Comparison of singlet oxygen production between a 4× serial concentration of porphyrin azide (156, 625, and 2500 nM) and 625 nM 7B2-porphyrin DAR4 (containing 2500 nM porphyrin in the interaction with 625 nM antibody). The graph shows that the ability of porphyrin to produce singlet oxygen has decreased after conjugation. The changes in ABDA absorption at 400 nm were measured as a function of irradiation time (0−50 min) on the generation of singlet oxygen by porphyrin azide in comparison to porphyrin−antibody (n = 3). (b) The changes in ABDA absorption at 400 nm during 50 min irradiation due to singlet oxygen generation by porphyrin-7B2 and IR700-7B2. IR700-PIC with DAR of 3 produced more singlet oxygen than the porphyrin-PIC (DAR: 4) in the aqueous solution. Singlet oxygen generation by PICs was quenched in the presence of 0.01% sodium azide. Data are mean ± SEM (n = 3) with two individual experiments. The controls include 7B2 and DD water (n = 3). (c) Photobleaching of UV−vis absorbance spectra of ABDA upon 40 min irradiation in the presence of PICs. The extra absorption bands are due to either IR700 or porphyrin, as the absorption band of porphyrin was quenched during irradiation, while the IR700 was preserved. The controls include 7B2 and DD water (n = 3).

antibody internalization due to the cytostatic effect but also inhibits the singlet oxygen-induced cell death. In this study, to avoid unwanted cell death due to the toxicity of azide,[29] we applied the minimum concentration of sodium azide (1.5 mM) with efficacy for $^1O_2$ quenching (Figure 4). This concentration differs with the applied concentrations ([NaN_3] = 10 or 50 mM) in the studies published elsewhere.[28,30]

Flow cytometric analysis demonstrated the percentage of cell death treated by 7B2 MAb or PICs. PIC-internalized model contains both intracellular and extracellular PICs, which can kill the cells via two mechanisms of apoptosis and membrane-damage necrosis. However, IR700-7B2 with a DAR of 3 showed more cytotoxicity than porphyrin-7B2. In the PIC membrane-localized model, porphyrin-7B2, IR700-7B2 DARs 2 and 3 showed 40%, 48%, and 51% cell death, although this cytotoxicity was inhibited by sodium azide due to the quenching of singlet oxygen (red arrows in Figure 4a). Parallel experiments with IR700-7B2 also showed cytotoxicity inhibition by sodium azide. Therefore, the presence of PICs on the cell membrane was sufficient to kill cells through singlet oxygen generation (which was confirmed by preventing cell death via quenching of singlet oxygen by azide). No significant cell death was observed for transfected cells treated by isotype controls or 293T control cells treated by PICs. These observations signify the role of singlet oxygen in the physical changes of the PIC−antigen complex on the cell membrane, resulting in membrane damage and cell necrosis. This kind of singlet oxygen-induced cell death is independent of the type of PSs (type I or II) or the charge of PSs (cationic porphyrin or anionic IR700), as the PSs are conjugated to the antibody. This also suggests a different mechanism for PIT as compared to conventional PDTs that depend on particular PSs and production of type I radicals or type II singlet oxygen.[31]

Live two-photon (2P) microscopy was performed to visualize the cellular binding locations of the porphyrin-7B2 during 2P irradiation at 800 nm. The cells were incubated with 7B2-porphyrin in PBA to block internalization (Figure 5a). In the absence of azide (Figure 5b, orange curve), the presence of

https://doi.org/10.1021/acsomega.1c01721
ACS Omega XXXX, XXX, XXX−XXX

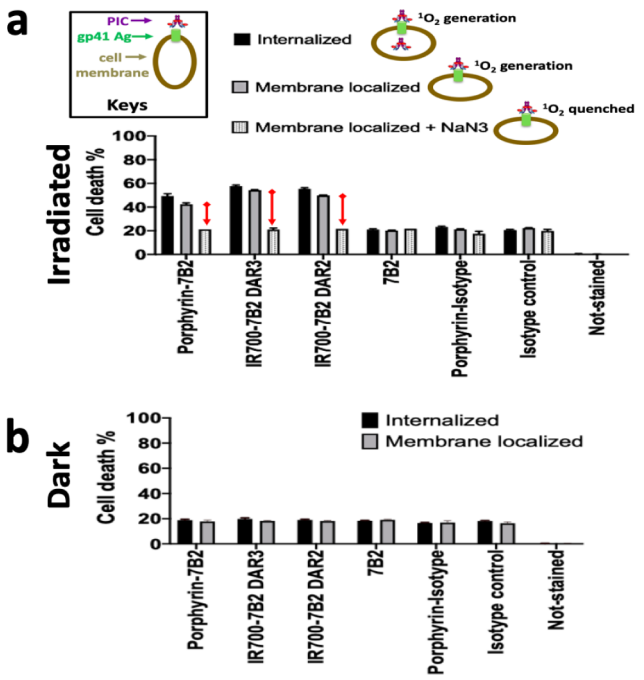

Figure 4. (a) Schematic picture depicts three models of PIC localization on the HIV Env-transfected 293T cell membrane or internalized. The irradiation was applied in the presence or absence of sodium azide as a $^1O_2$ quencher. The controls include unstained cells, the cells incubated with naked 7B2 antibody, mouse IgG1 isotype control, and porphyrin isotype. Parallel studies were performed on the cells in darkness (b) and control 293T cells (Figure S2). Red arrows indicate that the cell death was inhibited due to quenching of singlet oxygen by azide, indicating that the presence of PICs on the cell membrane is sufficient to kill the cells by singlet oxygen generation. All PIT treatments on transfected cells were in the presence of 5 μg/mL soluble CD4 (n = 3).

porphyrin-7B2 on the cell membrane was sufficient to damage the membrane, causing the internalization of porphyrin-7B2 as well as FITC secondary antibody after 10 min irradiation and inducing necrotic signs such as cellular swelling and bleb formation following 30 min irradiation (Figure 5c). In agreement with the singlet oxygen-induced phototoxicity results (Figure 4), neither membrane damage nor internalization was observed during irradiation in the presence of azide as a $^1O_2$ quencher. The mirror controls in darkness and 7B2 antibody alone did not show a significant percentage of cell death (Figure 5c).

We have shown before that the HIV ITs may kill the infected cells, with only neutralizing effect on the HIV, as the ITs need to internalize to kill the target via apoptosis.[15,17,32] Herein, we investigate whether the aforementioned PICs might cause necrotic cell death without internalization and whether this may lead to the potential ability of the PICs to destroy the HIV as well.

2.4. Viral Photoinactivation. Virus photoinactivation of the PICs was studied using two HIV-1 strains, X4 HIV-1 NL4-3 and JR-CSF virus, that utilize the CXCR4 coreceptor on Jurkat cells and CCR5 coreceptor on C8166.R5 cells, respectively. These CD4+ T-cell lines not only differ in cell surface expression of coreceptors but also in their permissiveness for infection.[33] The qPCR assay (Figure 6a,b) and p24 antigen ELISA assay (Figure S3) were done using less permissive Jurkat cells and high permissive C8166.R5 cells, respectively.

In the first study, treating the X4 NL4-3 virus with PIT at 500 nM of either PSs or PICs demonstrated undetectable levels of viral RNA load ($\log_{10}$ copies/mL) (Figure 6a) and proviral DNA load (HIV DNA copies/100 cell) in each region of HIV-1 LTR (Figure 6b). The results of PIT treated with non-neutralizing 7B2 antibody with 0.95 copies/mL RNA virus showed a significant decrease in viral replication, but this was still detectable, compared to the irradiated virus-only with 2.34 copies/mL. PIT-treated virus by porphyrin isotype showed about 10% decrease in viral load compared to isotype control, due to the singlet oxygen generation nearby (but not bind to) virion.[34] In the dark plate, samples treated with 7B2 MAb or PICs showed some decrease in the viral load due to the non-neutralizing binding of the antibody on the gp41 of the virus,[27] while PSs did not show virus inactivity in the absence of light (Figure 6a).

The morphology of untreated and PIT-treated X4 NL4-3 virus was examined using transmission electron microscopy (TEM). There were no differences in viral morphology between untreated virions or light and dark controls (Figure 6c). In contrast to the controls, virions irradiated with PICs or PSs showed different morphological changes depending upon the treatment type. The virions irradiated with 500 nM of IR700 dye showed multiple valence particle agglomerates. In contrast, the other PIT-treated samples showed the maintenance of membrane structural integrity or partially destroyed membranes with no agglomeration (Figure 6d). No change was observed in the level of surface glycoproteins. Despite virus inactivation by PIT, TEM images revealed minor membrane damages with no virion disintegration, presumably due to the oxidization of viral surface glycoproteins by singlet oxygen generation nearby the virus envelope (Figure 6d).[34]

In the second study using JR-CSF virus, the results of p24 ELISA were in agreement with HIV RNA viral load results from the first study. In the irradiated plate, the results for PIC-treated samples showed a significant decrease in p24 production, in comparison to the mirror samples in darkness. In the dark plate, the samples treated with 7B2 MAb or PS antibodies showed some decline in p24 production, as 7B2 MAb binds HIV-1 Env but fails to neutralize the virus completely. On day 3, irradiation with 20 J/cm^2 of light (380–780 nm) on the untreated viruses has an inhibition effect on the transfection (Figure S3a). However, this is not considered a long-term inhibition as the viral load increases for the irradiated viruses on day 4 compared to the untreated viruses in darkness. The results revealed that the maximum photoinactivity was achieved only when HIV-1 strain JR-CSF virus was treated with PIC and exposed to light (Figure S3b).

Therefore, we showed that neither X4 HIV-1 NL4-3 nor JR-CSF virus could infect the target cells after PDT with PICs or PSs, demonstrating that the virus inactivity is neither dependent on the PS type (cationic and anionic) nor dependent on the viral internalization. Current limitations in microscopic studies make it difficult to visualize molecular changes on the HIV envelope. We suggest further studies using advanced microscopy to understand the role of ROS-dependent toxicity in hypoxic conditions,[34] as well as the photochemical reaction of PSs alone[35−37] and in the PS–antibody structure[21,38] in virus inactivation.

As a scenario to obtain the HIV cure, we previously studied ART-suppressed individuals associated with latency reversal

https://doi.org/10.1021/acsomega.1c01721
ACS Omega XXXX, XXX, XXX−XXX

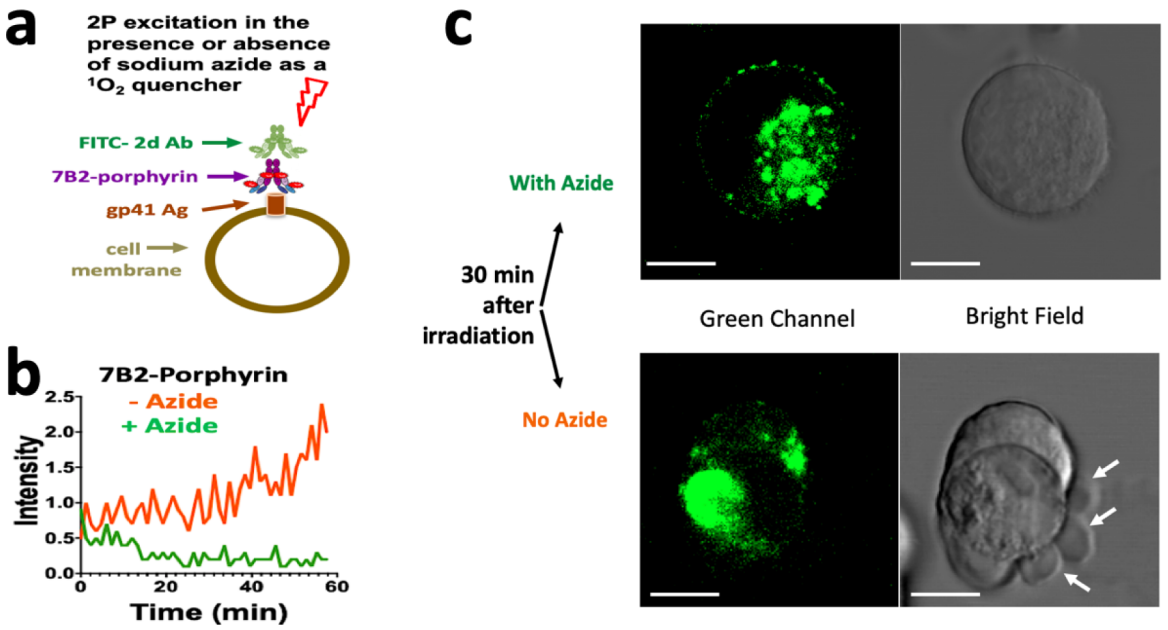

Figure 5. (a) Schematic picture depicts the model of study for comparing the cell internalization of porphyrin−antibody during 2P irradiation in the presence or absence of azide. (b and c) The cells were incubated with 7B2-porphyrin in PBA to block internalization. FITC anti-human IgG secondary antibody was added to detect 7B2-porphyrin. After three washes with PBS, the cells were irradiated at 800 nm. In the absence of azide, membrane damage and rapid internalization of porphyrin−antibody were observed in 10 min (b, orange curve), resulting in necrotic signs after 30 min irradiation (c). In contrast, neither membrane damage nor internalization was observed during 60 min irradiation in the presence of azide as a $^1O_2$ quencher (b, green curve). The white bar indicates 10 μm.

inhibitors.[39,40] The long-term ART sometimes poses harm to human health due to the toxicity of drugs that may inhibit proteases,[41] some human polymerases, or even disrupt the respiratory cell cycle.[42] PIT is potentially less toxic and may add potency and increase the genetic barrier of current ART when used in association with currently used drugs. If proven effective in vivo, PIT associated with ART may be used with a lower number of antiretroviral drugs to decrease the long-term toxicity of these drugs. However, one unknown issue about PIT is the emergency of virus or cell resistance, a paradigm of antiretroviral treatment. The use of PIT and ART, which may decrease HIV replication substantially, might mitigate the risk of PIT resistance.

3. CONCLUSIONS

HIV-infected cells persist and are cleared from the body extremely slowly, despite decades of ART on a life-long basis,[1] preventing the complete elimination of HIV in a person's lifetime. Meanwhile, HIV drug resistance to ART is a serious threat to the global scale-up of HIV treatment.[3] Several IT strategies, using armed antibodies specific to virus Env, have been investigated to activate the apoptotic pathway to kill latently infected cells.[12,43] But these ITs are dependent on cell internalization and not able to destroy the HIV virus.

This study showed that the excited PSs (porphyrin and IR700) within the PS−antibody construct may cause antibody aggregation. When PICs bound to HIV Env on the cell membrane, the physical changes in the structure of irradiated PS−antibody may damage the membrane and result in necrotic cell death without internalization. We showed that the singlet oxygen has a pivotal role in this reaction. This finding persuaded us to study the possibility of destroying HIV using PICs (graphical picture). Targeted phototoxicity on both HIV strains and HIV-infected cells is a possible dual combination for ART, including treatment for antiretroviral drug-resistant HIV strains. More importantly, as specialized noninvasive IT to kill HIV-infected cells and eradicate persistent reservoirs of HIV infection and potentially destroy HIV due to residual viral replication, PICs may constitute a fundamental tool for HIV cure. This mechanism may mitigate HIV-related microinflammation and/or obtain HIV remission without antiretrovirals. Furthermore, these strategy's results can potentially translate to viral PIT against other enveloped viruses with similar mechanisms of viral replication, such as HBV and HTLV, which cause still incurable chronic infections.

4. MATERIALS AND METHODS

4.1. Chemical Reagents. All reagents are from Thermo-Fisher Scientific (Waltham, MA, USA), unless otherwise stated.

4.2. Cells and Viruses. 293T cell lines stably express clade A clinical isolate 92UG037.8 gp160 as native gp120/gp41trimers (293T/92UG).[44] 293T cells were used as uninfected control cells. The transfected and nontransfected 293T cells were maintained at 37 °C in 5% CO_2 in DMEM medium with 10% fetal bovine serum (Gibco Invitrogen, Grand Island, NY, USA). In this paper, Env-transfected cells refer to the 293T cells stably transfected with 92UG037.8 gp160.

Highly permissive C8166.R5 cells are CD4+ lymphoma cells that have been transfected to express CCR5 coreceptors.[33] Jurkat cell line (Clone E6-1) are CD4+ human T lymphocyte cells with cell surface expression of CXCR4 coreceptors. The cells were kindly provided by Dr. David Kabat.[45]

HIV-1 JR-CSF virus is a group M, lab-adapted variant, which utilizes CCR5 as a coreceptor.[46] HIV1 NL4-3 is also a group M variant but uses the CXCR4 as a coreceptor.[17,47]

https://doi.org/10.1021/acsomega.1c01721
ACS Omega XXXX, XXX, XXX−XXX

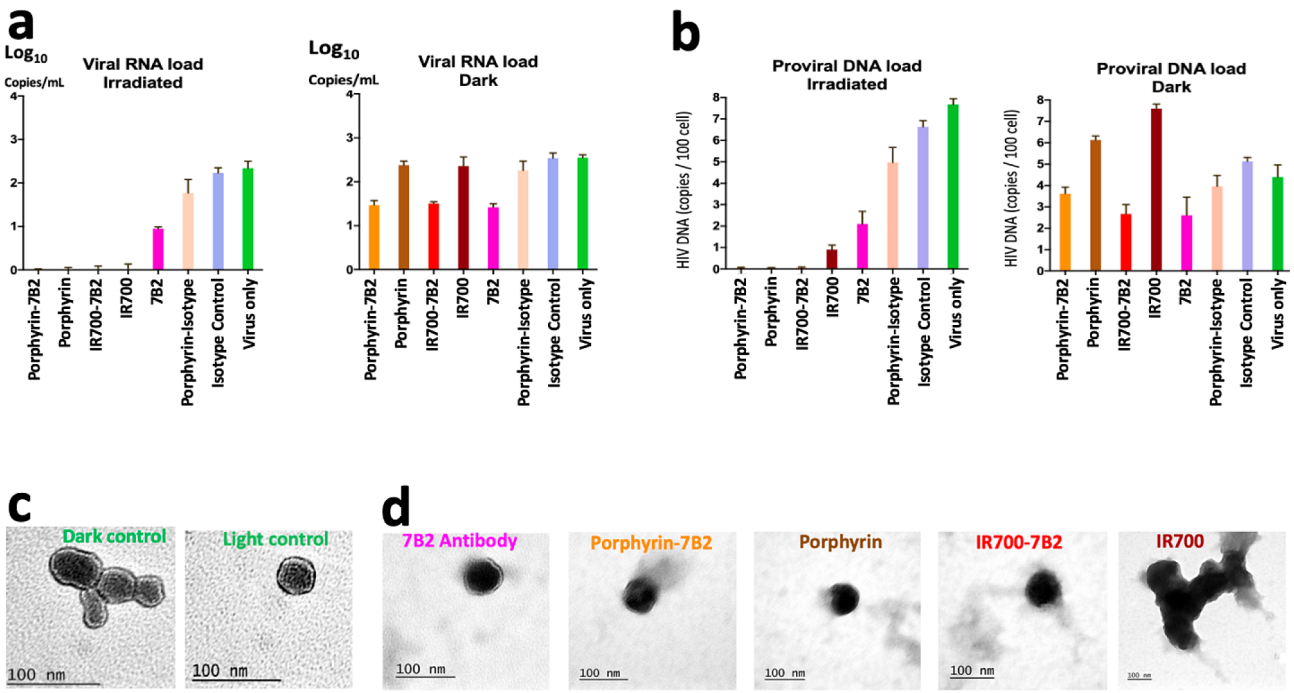

Figure 6. Effect of PICs on X4 HIV-1 NL4-3 virus. The virus stock was incubated with 500 nM of PICs, PSs, anti-gp41 (7B2) naked MAb, mouse IgG1 isotype control, porphyrin isotype, and wells with no treatment (only virus). After irradiation, the Jurkat cells were infected with viruses. (a) HIV-1 RNA load (log_{10} copies/mL) in each region of LTR from harvested supernatants on day 6. In the irradiated plate, the viral load was undetectable in the samples treated with PICs or PSs. In the dark plate, the samples treated with naked 7B2 MAb or PS antibodies showed a decrease in the viral load due to the non-neutralizing binding of 7B2 MAb on the gp41 of the virus. Data were subtracted from HIV stock (log_{10} copies/mL). Data are mean ± SEM (n = 2) for the supernatant of day 6. (b) Quantification of HIV-1 proviral DNA load (HIV DNA copies/100 cells) based on the protocol of Kumar for amplification of region LTR of the virus. Total HIV DNA includes stably integrated proviruses and extrachromosomal HIV DNA forms. The results were in agreement with viral RNA load results. Data are mean ± SEM (n = 2) for the supernatant of day 3. (c) TEM images of dark and irradiated controls revealed that the near-spherical enveloped virions look intact with distinct envelope. (d) The morphology of the virions irradiated with naked 7B2 antibody showed no difference with the untreated controls. While the membrane of virions inactivated with porphyrin, porphyrin−antibody, or IR700−antibody became partially destroyed, but their membranes appeared to maintain structural integrity. PIT-treated virions with IR700 PS were mostly agglomerated.

4.3. Antibodies. MAb 7B2 (Genbank accession nos. JX188438 and JX188439) is a human IgG1 that binds HIV gp41 at AA 598−604 (CSGKLIC) in the helix−loop−helix region.[24,48] MAb 7B2 is a non-neutralizing antibody that recognizes both virus particles and infected cells. The following isotype controls were used: Mouse IgG1 kappa Isotype Control, clone P3.6.2.8.1 (eBioscience, Inc., San Diego, CA, USA), and HY (Genbank accession nos. JX188440 and JX188441), an affinity matured version of the anti-CD4 binding site Ab b12.[49] MAbs were purified from hybridoma supernatant on Protein A agarose beads (Invitrogen, Carlsbad, CA, USA) and eluted with 0.1 M glycine, pH 2.5, immediately neutralized, and dialyzed vs PBS. Two types of soluble CD4 were used to observe CD4-mediated effects;[48] CD4-183 contains the first two domains of CD4, including the region in domain 1 that binds the HIV coat protein gp120. CD4-IgG2 is a tetrameric fusion protein comprising human IgG2 in which the Fv portions of both heavy and light chains have been replaced by the V1 and V2 domains of human CD4. Goat anti-human IgG (Invitrogen) was conjugated to either alkaline phosphatase (AP) or fluorescein isothiocyanate (FITC).

4.4. Porphyrin−Antibody Conjugation by Click Chemistry. Conjugation between azide porphyrin and 7B2 antibody or mouse IgG1 isotype control was carried out in two steps: antibody functionalization and then click chemistry conjugation. The process is a modification of our protocol described previously.[20,50,51]

4.5. Conjugation and Optimization of IR700−Antibody by Lysine Modification. IRDye 700DX (IR700, LI-COR Biosciences, Lincoln, NE, USA) was conjugated with 7B2 antibody via Lys modification through an *N*-hydroxysuccinimide reactive group, according to the manufacturer's instructions.[25] The process is a modification of our protocol described previously.[20]

4.6. UV−Vis Spectroscopy. UV−vis spectroscopy was used to determine protein concentrations and PS-to-antibody ratios, first using a Nanodrop 1000 UV−visible spectrophotometer (ThermoFisher Scientific, Waltham, MA, USA) and then a Varian Cary 100 Bio UV−visible spectrophotometer (Varian, CA, USA) operating at 21 °C. A correction factor at 280 nm of 0.25 (at A_{335}) was employed for pyridazinedione scaffolds, as described elsewhere.[52]

4.7. Electrophoresis. Molecular size, purity, and accuracy of the conjugation of products were determined before and after irradiation with 50 J/cm^2 using nonreducing glycine-SDS-PAGE and then confirmed by microcapillary electrophoresis (Agilent Bioanalyzer, GE Healthcare, Piscataway, NJ, USA), following standard lab procedures.

4.8. ELISA. ELISAs were performed for Ag-binding specificity analysis and titration of purified MAbs and PICs in wells coated with gp41 antigen (1 μg/mL), as described elsewhere.[32] The gp41 antigen was a linear peptide HIV-1 consensus clade B sequence [LGIWGCSGKLICTT] representing the epitope of 7B2. Binding of antibody to the antigen

https://doi.org/10.1021/acsomega.1c01721
ACS Omega XXXX, XXX, XXX−XXX

was detected with AP-conjugated secondary antibody (goat anti-human IgG) (Zymed Laboratories, South San Francisco, CA, USA). To study the effect of irradiation on the binding ability of PICs, the ELISAs were performed in two models; PICs were kept in the dark during the experiment as a mirror control or irradiated with 50 J/cm^2 before incubation with gp41. Mouse IgG1 was used as an isotype control. Data are reported as optical density at 405 nm and represent means of triplicate values with three independent experiments.

4.9. Dynamic Light Scattering. Hydrodynamic radii, electrophoretic mobility, zeta potential, and polydispersity of naked antibody and PICs were measured before and after conjugation, as well as PICs irradiated with 50 J/cm^2. Samples with 70 μL volume at 1 mg/mL in UV-transparent 96-well plates were measured using a DLS Wyatt Möbius (Wyatt Technologies, Dernbach, Germany) with incident light at 532 nm, at an angle of 163.5°. Samples were equilibrated at 25 ± 0.1 °C for 600 s before the measurements, and this temperature was held constant throughout the experiments. All samples were measured in triplicate with 10 acquisitions and a 5 s acquisition time. The change in cumulant fitted hydrodynamic radius in nanometers was monitored during the storage period. The results were calculated using the Dynamics 7.1.7 software (Wyatt Technologies, Santa Barbara, CA, USA). Previously, using an Agilent Technologies Cary 5000 Series UV−vis−NIR spectrofluorimeter (Agilent Bioanalyzer, GE Healthcare, Piscataway, NJ, USA), we showed the incident laser beam at 532 nm is not within the fluorescent sample's (IR700-7B2 and porphyrin-7B2) band of excitation; as the analysis would not be disrupted or tainted.[27]

4.10. Singlet Oxygen Generation in the Media. Singlet oxygen generation was evaluated by photobleaching the chemical probe 9,10-anthracenediyl-bis(methylene)dimalonic acid (ABDA) (purchased from Sigma-Aldrich). The singlet oxygen produced by a range of concentrations of PICs in 0.15 mM of the sodium salt of ABDA in water was thus determined. PICs were incubated in the presence or absence of 0.01% sodium azide. After time-controlled irradiation (380−750 nm) by LED array (30 mW/cm^2), the decrease in absorption at 400 nm (λ_{max} of ABDA) as well as the UV−vis spectra of ABDA + PIC was measured with an Agilent Technologies Cary Series UV−vis−NIR spectrophotometer (Cary 5000). The experiments were also carried out without photostimulation. A control consisting of the ABDA solution without PICs irradiated under the same conditions was analyzed in parallel.

4.11. Singlet Oxygen-Induced Phototoxicity by Flow Cytometry. We studied the phototoxicity of PICs in three models of PIC-localization: the internalized PICs and the membrane-binding models in the presence and absence of sodium azide as a $^1O_2$ quencher. All PIT treatments were performed in the presence of 5 μg/mL soluble CD4. Mouse IgG1 in naked and porphyrin-conjugated forms were used as isotype controls.

For the internalized model, the incubation and irradiation were done in absence of sodium azide. Env-transfected 293T cells were incubated with 10 μg/mL MAbs/PICs for 1 h, washed twice to remove unbound PICs, and then irradiated in DMEM media without phenol red with 20 J/cm^2 of light (380−780 nm) by a homemade LED array (30 mW/cm^2).

For the membrane-binding models, to block the PIC internalization, the cells were incubated with PBA (PBS/1% BSA/0.01% sodium azide) for 30 min and then treated with 10 μg/mL MAbs/PICs for 1 h in RT. The cells were washed twice to remove unbound PICs, irradiated with 20 J/cm^2 of light (380−780 nm) in the presence and absence of sodium azide, as a singlet oxygen quencher.

Fifteen minutes before flow cytometry measurement, the cells were stained with 2 μg/mL of propidium iodide (Life Technologies, Carlsbad, CA, USA) as an indicator of cell death. PIT-treated cells (10 000) were studied on Accuri C6 (Accuri Cytometers, Ann Arbor, MI, USA), analyzed by FlowJo software version 7.5 (Tree Star, Inc., Ashland, OR, USA). Mean fluorescence of the gated cell population labeled with immunoconjugate was calculated in relation to the mean fluorescence of cells labeled with MAb 7B2. The process of preparing models based on the PIC-localization is described in a table in Figure S1. A paralleled study was performed on control 293T cells (Figure S2).

4.12. Live Imaging by 2P Confocal Microscopy. First, the cells were incubated with PBS/BSA/0.01% sodium azide (PBA) to inhibit any PIC internalization. Afterward, the cells were treated with 10 μg/mL porphyrin-7B2 and 5 μg/mL soluble CD4 for 1 h in PBA, then washed, and stained with FITC-conjugated goat anti-human IgG secondary antibody (2 μg/mL) for 1 h in PBA. The cells were irradiated by 2P excitation at 800 nm (2.2 mW/cm), the presence or absence of sodium azide (PBA or PBS) (see schematic picture in Figure 5a).

Live cell imaging was performed using a Zeiss LSM 780 confocal inverted microscope (Zeiss, Jena, Germany) with a Coherent Chameleon laser (Ti:sapphire, Coherent, Santa Clara, CA, USA) as a source for 2P excitation at 800 nm. The images were obtained by the average of two scans, and no appreciable variation was observed. Live imaging was performed based on the time-series experiment consisting of image sequences with time intervals of 30 s, and the nominal light dose delivered for each image pixel was 1 J/cm^2. The spatial resolution was approximately 250 nm (considering the numerical aperture and the wavelength of excitation), as described previously.[53]

4.13. HIV Photoinactivity. Two HIV-1 strains, X4 HIV-1 NL4-3 and JR-CSF virus, were used to study the photoinactivity assay on Jurkat cells and C8166.R5 cells, respectively.

Virus stocks of X4 HIV-1 NL4-3 or JR-CSF virus were diluted in 100 μL phenol-free RPMI without FCS in triplicate wells, then were treated at 37 °C for 45 min with 500 nM of PICs, PSs, anti-gp41 (7B2) naked MAb, mouse isotype controls in naked and porphyrin-conjugated forms, and three wells with no treatment. A mirror plate was incubated and kept in darkness, as not-irradiated control. The plate was irradiated with 20 J/cm^2 of light (380−780 nm) by a custom-made LED array (30 mW/cm^2) in two equal doses separated by 10 min, as described elsewhere.[49,50] Afterward, 120 μL RPMI media with 20% FCS was added to each well, and the plates were returned to the incubator. At 30 min after irradiation, a serial concentration of Jurkat cells or C8166.R5 cells with the order of 10^7, 10^6, and 10^5 cell/mL were added into the triplicate wells containing 500 μL final volume of irradiated X4 HIV-1 NL4-3 or JR-CSF virus, respectively. This order of final concentrations was representing the specific multiplicity of infection (MOI) of 0.1, 1, and 10. The cells were incubated for 6 days, while 50 μL of sample was harvested per day, and centrifuged. The pellets of Jurkat cells were harvested for proviral DNA qPCR, and the supernatants were harvested for viral RNA. In contrast, the supernatants of C8166.R5 cells were harvested for p24 antigen assay.

https://doi.org/10.1021/acsomega.1c01721
ACS Omega XXXX, XXX, XXX−XXX

4.14. Quantification of HIV-1 Viral RNA. Total HIV-1 RNA from the supernatant of samples in day 6 with MOI of 1 was extracted and purified using the RNeasy Lipid Tissue Mini Kit, according to the manufacturer's (QIAGEN) protocol. HIV-1 viral load measurement was carried out using one-step reverse transcriptase (RT) and real-time PCR in a single buffer system using the Abbott RealTime HIV-1 on the automated m2000, over the dynamic range of detection of 40 to 10 000 000 copies/mL (Abbott, IL, USA). The protocol was followed as described by the vendor (Applied Biosystems) for the TaqMan one-step RT and PCR Master Mix Reagents Kit (Thermo Fisher Scientific, MA, USA).[54]

4.15. Quantification of HIV-1 Proviral DNA by the TaqMan Real-Time PCR Assay. The number of Jurkat cells containing proviral DNA of HIV-1 was measured using qPCR. The harvested samples of day 3 were centrifuged and the pellets were separated. The quantification was done based on two distinct previously published protocols[55,56] for amplification of proviral DNA of HIV-1 (region LTR) as well as the amplification of CCR5 to measure the total cells.

4.16. Electron Microscopy. TEM analysis was conducted to assess the morphology of untreated and PIT-treated HIV-1 NL4-3 virus, as described in Section 4.13. Then, the residual virions were fixed using 0.1% paraformaldehyde for 15 min at 4°C. Samples were subjected to negative staining as previously described[57] with a few modifications. The uranyl acetate grids were placed onto 30 μL of samples for 10 min. Staining was carried out by 2% potassium phosphotungstate (pH 7.2). The grids were observed under a JEOL TEM (model JEM1011) (JEOL/Massachusetts/USA) operating at 80 kV. Images were recorded with a charged-couple device camera (model 785 ES1000W, Gatan, USA) and the Gatan version 1.6 program.

4.17. Statistical Analyses. Statistical analyses were performed using GraphPad Prism version 8.0 (GraphPad Software, San Diego, CA, USA). Data are shown as mean and SEM of the indicated number of replicate values. If no error bar appears, the error bars are smaller than, and obscured by, the symbol. The method for statistical comparison is the unpaired two-tailed Student *t* test, unless specifically indicated otherwise.

4.18. Data Availability. All data generated or analyzed during this study are included in this article and its Supporting Information.

■ ASSOCIATED CONTENT

Supporting Information

The Supporting Information is available free of charge at https://pubs.acs.org/doi/10.1021/acsomega.1c01721.

> Schematic pictures and table depict the process of preparing PIT-treated cells in three models (Figure S1); study of the phototoxicity of PICs on 293T control cells not expressing gp41 (Figure S2); and effect of PICs on HIV-1 strain JR-CSF virus (Figure S3) (PDF)

■ AUTHOR INFORMATION

Corresponding Author

Ricardo Sobhie Diaz − *Laboratório de Retrovirologia, Universidade Federal de São Paulo, São Paulo, Brazil;* orcid.org/0000-0002-8395-7304; Email: rsdiaz@catg.com.br; Fax: +55-11-91090445

Authors

Mohammad Sadraeian − *São Carlos Institute of Physics, São Carlos, SP CEP 13560-970, Brazil;* orcid.org/0000-0002-7384-2247

Edgar Ferreira da Cruz − *Laboratório de Retrovirologia, Universidade Federal de São Paulo, São Paulo, Brazil*

Ross W. Boyle − *Department of Chemistry, University of Hull, Hull HU6 7RX, U.K.;* orcid.org/0000-0001-7476-9857

Calise Bahou − *Department of Chemistry, University College London, London WC1H 0AJ, U.K.*

Vijay Chudasama − *Department of Chemistry, University College London, London WC1H 0AJ, U.K.;* orcid.org/0000-0002-8876-3285

Luiz Mário Ramos Janini − *Laboratório de Retrovirologia, Universidade Federal de São Paulo, São Paulo, Brazil*

Francisco E. G. Guimarães − *São Carlos Institute of Physics, São Carlos, SP CEP 13560-970, Brazil*

Complete contact information is available at: https://pubs.acs.org/10.1021/acsomega.1c01721

Author Contributions

R.S.D., F.E.G.G., and M.S. wrote the main manuscript text and prepared the figures. F.E.G.G., R.W.B., V. C., and M.S. designed and performed the biochemical, immunological, and microscopy experiments. R.S.D., E.F.C., M.S., and L.M.R.J. designed and performed the viral assays. C.B. performed the small molecule synthesis and performed the bioconjugation experiments. R.S.D. and F.E.G.G. supervised the study. All authors reviewed the manuscript.

Funding

The authors acknowledge the support provided by the FAPESP (Sao Paulo Research Foundation) under grant #645 2017/10 910-5 (M.S. Pós-Doutorado-Fluxo Contínuo), #2013/07276-1 (CEPOF-CEPID Program), #2009/54 647 035-4 (EMU), #2013/11323-5 (RD); and CNPq (Brazilian National Research Council) grant #454700-2014-8 (RD) and #441817/2018-1 (RD). The reagents related to HIV were supported by the NIH AIDS Research and Reference Reagent Program. The authors also gratefully acknowledge the Leverhulme Trust (RPG-2020-010) for funding C.B.

Notes

The authors declare the following competing financial interest(s): V.C. is a Director of ThioLogics. Other authors declare no competing interests.

■ ACKNOWLEDGMENTS

We thank Seth Pincus for his support in the Department of Chemistry and Biochemistry, Montana State University, Bozeman, MT. We thank Juliana Galinskas (Unifesp) for her valuable expertise in the quantification assay.

■ ABBREVIATIONS

ART	antiretroviral therapy
IT	immunotherapy
DAR	drug−antibody ratio
MAb	monoclonal antibody
PDT	photodynamic therapy
PIT	photoimmunotherapy
PS	photosensitizer
ROS	reactive oxygen species
TEM	transmission electron microscopy

https://doi.org/10.1021/acsomega.1c01721
ACS Omega XXXX, XXX, XXX−XXX

REFERENCES

(1) Davenport, M. P.; Khoury, D. S.; Cromer, D.; Lewin, S. R.; Kelleher, A. D.; Kent, S. J. Functional Cure of HIV: The Scale of the Challenge. *Nat. Rev. Immunol.* **2019**, *19*, 45−54.

(2) Ndung'u, T.; McCune, J. M.; Deeks, S. G. Why and Where an HIV Cure is Needed and How it might be Achieved. *Nature* **2019**, *576*, 397−405.

(3) World Health Organization (WHO). *HIV Drug Resistance Report*, 2019.

(4) Zhang, Z.; Li, S.; Gu, Y.; Xia, N. Antiviral Therapy by HIV-1 Broadly Neutralizing and Inhibitory Antibodies. *Int. J. Mol. Sci.* **2016**, *17*, 1−12.

(5) Bertrand, L.; Méroth, F.; Tournebize, M.; Leda, A. R.; Sun, E.; Toborek, M. Targeting the HIV-infected brain to improve ischemic stroke outcome. *Nat. Commun.* **2019**, *10*, No. 2009.

(6) Palmer, S.; Maldarelli, F.; Wiegand, A.; Bernstein, B.; Hanna, G. J.; Brun, S. C.; Kempf, D. J.; Mellors, J. W.; Coffin, J. M.; King, M. S. Low-Level Viremia Persists for at Least 7 Years in Patients on Suppressive Antiretroviral Therapy. *Proc. Natl. Acad. Sci. U. S. A.* **2008**, *105*, 3879−3884.

(7) Anton, P. A.; Mitsuyasu, R. T.; Deeks, S. G.; Scadden, D. T.; Wagner, B.; Huang, C.; Macken, C.; Richman, D. D.; Christopherson, C.; Borellini, F.; Lazar, R.; Hege, K. M. Multiple Measures of HIV Burden in Blood and Tissue are Correlated with Each Other but Not with Clinical Parameters in Aviremic Subjects. *AIDS* **2003**, *17*, 53−63.

(8) Maldarelli, F. HIV-Infected Cells are Frequently Clonally Expanded after Prolonged Antiretroviral Therapy: Implications for HIV Persistence. *J. Virus Erad.* **2015**, *1*, 237−244.

(9) Samer, S.; Namiyama, G.; Oshiro, T.; Arif, M. S.; Cardoso Da Silva, W.; Sucupira, M. C. A.; Janini, L. M.; Diaz, R. S. Evidence of Noncompetent HIV after Ex Vivo Purging among ART-Suppressed Individuals. *AIDS Res. Hum. Retroviruses* **2017**, *33*, 993−994.

(10) Imamichia, H.; Dewar, R. L.; Adelsberger, J. W.; Rehm, C. A.; O'doherty, U.; Paxinos, E. E.; Fauci, A. S.; Lane, H. C. Defective HIV-1 proviruses produce novel protein-coding RNA species in HIV-infected patients on combination antiretroviral therapy. *Proc. Natl. Acad. Sci. U. S. A.* **2016**, *113*, 8783−8788.

(11) Diaz, R. S.; Shytaj, I. L.; Giron, L. B.; Obermaier, B.; Della Libera, E.; Galinskas, J.; Dias, D.; Hunter, J.; Janini, M.; Gosuen, G.; Ferreira, P. A.; Sucupira, M. C.; Maricato, J.; Fackler, O.; Lusic, M.; Savarino, A. Potential Impact of the Antirheumatic Agent Auranofin on Proviral HIV-1 DNA in Individuals under Intensified Antiretroviral Therapy: Results from a Randomised Clinical Trial. *Int. J. Antimicrob. Agents* **2019**, *54*, 592−600.

(12) Caskey, M.; Klein, F.; Nussenzweig, M. C. Broadly Neutralizing Anti-HIV-1 Monoclonal Antibodies in the Clinic. *Nat. Med.* **2019**, *25*, 547−553.

(13) Parsons, M. S.; Le Grand, R.; Kent, S. J. Neutralizing Antibody-Based Prevention of Cell-Associated HIV-1 Infection. *Viruses* **2018**, *10*, 1−13.

(14) Qiao, Z.; Li, X.; Kang, N.; Yang, Y.; Chen, C.; Wu, T.; Zhao, M.; Liu, Y.; Ji, X. A Novel Specific Anti-Cd73 Antibody Inhibits Triple-Negative Breast Cancer Cell Motility by Regulating Autophagy. *Int. J. Mol. Sci.* **2019**, *20*, 1057.

(15) Pincus, S. H.; Song, K.; Maresh, G. A.; Hamer, D. H.; Dimitrov, D. S.; Chen, W.; Zhang, M.; Ghetie, V. F.; Chan-Hui, P.-Y.; Robinson, J. E.; Vitetta, E. S. Identification of Human Anti-HIV Gp160 Monoclonal Antibodies That Make Effective Immunotoxins. *J. Virol.* **2017**, *91*, No. JVI.01955−16.

(16) Sadraeian, M.; Rasoul-Amini, S.; Mansoorkhani, M. J. K.; Mohkam, M.; Ghoshoon, M. B.; Ghasemi, Y. Induction of Antitumor Immunity against Cervical Cancer by Protein HPV-16 E7 in Fusion with Ricin B Chain in Tumor-Bearing Mice. *Int. J. Gynecol. Cancer* **2013**, *23*, 809−814.

(17) Sadraeian, M.; Guimarães, F. E. G.; Araújo, A. P. U.; Worthylake, D. K.; LeCour, L., Jr.; Pincus, S. H. Selective Cytotoxicity of a Novel Immunotoxin Based on Pulchellin A Chain for Cells Expressing Expressing HIV Envelope. *Sci. Rep.* **2017**, *7*, No. 7579.

(18) Sadraeian, M.; Khoshnood Mansoorkhani, M. J.; Mohkam, M.; Rasoul-Amini, S.; Hesaraki, M.; Ghasemi, Y. Prevention and Inhibition of TC-1 Cell Growth in Tumor Bearing Mice by HPV16 E7 Protein in Fusion with Shiga Toxin B-Subunit from *Shigella dysenteriae*. *Cell J.* **2013**, *15*, 176−181.

(19) Ponziani, S.; Di Vittorio, G.; Pitari, G.; Cimini, A. M.; Ardini, M.; Gentile, R.; Iacobelli, S.; Sala, G.; Capone, E.; Flavell, D. J.; Ippoliti, R.; Giansanti, F. Antibody-Drug Conjugates: The New Frontier of Chemotherapy. *Int. J. Mol. Sci.* **2020**, *21*, 1−28.

(20) Sadraeian, M.; Bahou, C.; Da Cruz, E. F.; Janini, L. M. R.; Diaz, R. S.; Boyle, R. W.; Chudasama, V.; Guimarães, F. E. G. Photoimmunotherapy Using Cationic and Anionic Photosensitizer-Antibody Conjugates against HIV Env-Expressing Cells. *Int. J. Mol. Sci.* **2020**, *21*, 1−16.

(21) Sandland, J.; Boyle, R. W. Photosensitizer Antibody-Drug Conjugates: Past, Present, and Future. *Bioconjug. Chem.* **2019**, *30*, 975−993.

(22) Butzbach, K.; Konhäuser, M.; Fach, M.; Bamberger, D. N.; Breitenbach, B.; Epe, B.; Wich, P. R. Receptor-Mediated Uptake of Folic Acid-Functionalized Dextran Nanoparticles for Applications in Photodynamic Therapy. *Polymers (Basel)* **2019**, *11*, 8−10.

(23) Tsukrov, D.; Dadachova, E. The Potential of Radio-immunotherapy as a New Hope for HIV Patients. *Expert Rev. Clin. Immunol.* **2014**, *10*, 553−555.

(24) Pincus, S. H.; Fang, H.; Wilkinson, R. A.; Marcotte, T. K.; Robinson, J. E.; Olson, W. C. In Vivo Efficacy of Anti-Glycoprotein 41, but Not Anti-Glycoprotein 120, Immunotoxins in a Mouse Model of HIV Infection. *J. Immunol.* **2003**, *170*, 2236−2241.

(25) Caudle, A. S.; Yang, W. T.; Mittendorf, E. A.; Kuerer, H. M. Cancer Cell-Selective In Vivo Near Infrared Photoimmunotherapy Targeting Specific Membrane Molecules. *Nat. Med.* **2016**, *150*, 137−143.

(26) Bryden, F.; Maruani, A.; Savoie, H.; Chudasama, V.; Smith, M. E. B.; Caddick, S.; Boyle, R. W. Regioselective and Stoichiometrically Controlled Conjugation of Photodynamic Sensitizers to a HER2 Targeting Antibody Fragment. *Bioconjug. Chem.* **2014**, *25*, 611−617.

(27) Santra, S.; Tomaras, G. D.; Warrier, R.; Nicely, N. I.; Liao, H. X.; Pollara, J.; Liu, P.; Alam, S. M.; Zhang, R.; Cocklin, S. L.; Shen, X.; Duffy, R.; Xia, S. M.; Schutte, R. J.; Pemble, C. W., IV; Dennison, S. M.; Li, H.; Chao, A.; Vidnovic, K.; Evans, A.; Klein, K.; Kumar, A.; Robinson, J.; Landucci, G.; Forthal, D. N.; Montefiori, D. C.; Kaewkungwal, J.; Nitayaphan, S.; Pitisuttithum, P.; Rerks-Ngarm, S.; Robb, M. L.; Michael, N. L.; Kim, J. H.; Soderberg, K. A.; Giorgi, E. E.; Blair, L.; Korber, B. T.; Moog, C.; Shattock, R. J.; Letvin, N. L.; Schmitz, J. E.; Moody, M. A.; Gao, F.; Ferrari, G.; Shaw, G. M.; Haynes, B. F. Human Non-Neutralizing HIV-1 Envelope Monoclonal Antibodies Limit the Number of Founder Viruses during SHIV Mucosal Infection in Rhesus Macaques. *PLoS Pathog.* **2015**, *11*, 1−38.

(28) Maisch, T.; Baier, J.; Franz, B.; Maier, M.; Landthaler, M.; Szeimies, R.-M.; Baumler, W. The Role of Singlet Oxygen and Oxygen Concentration in Photodynamic Inactivation of Bacteria. *Proc. Natl. Acad. Sci. U. S. A.* **2007**, *104*, 7223−7228.

(29) Jones, J. A.; Starkey, J. R.; Kleinhofs, A. Toxicity and mutagenicity of sodium azide in mammalian cell cultures. *Mutat. Res.* **1980**, *77*, 293−299.

(30) Mitsunaga, M.; Ogawa, M.; Kosaka, N.; Rosenblum, L. T.; Choyke, P. L.; Kobayashi, H. Cancer Cell-Selective in Vivo near Infrared Photoimmunotherapy Targeting Specific Membrane Molecules. *Nat. Med.* **2011**, *17*, 1685−1691.

(31) Debele, T. A.; Peng, S.; Tsai, H.-C. Drug Carrier for Photodynamic Cancer Therapy. *Int. J. Mol. Sci.* **2015**, *16*, 22094−22136.

(32) Craig, R. B.; Summa, C. M.; Corti, M.; Pincus, S. H. Anti-HIV Double Variable Domain Immunoglobulins Binding Both Gp41 and Gp120 for Targeted Delivery of Immunoconjugates. *PLoS One* **2012**, *7*, 1−13.

(33) Krowicka, H.; Robinson, J. E.; Clark, R.; Hager, S.; Broyles, S.; Pincus, S. H. Use of Tissue Culture Cell Lines to Evaluate HIV Antiviral Resistance. *AIDS Res. Hum. Retroviruses* **2008**, *24*, 957−967.

https://doi.org/10.1021/acsomega.1c01721
ACS Omega XXXX, XXX, XXX−XXX

(34) Davies, M. J. Reactive Species Formed on Proteins Exposed to Singlet Oxygen. *Photochem. Photobiol. Sci.* **2004**, *3*, 17−25.
(35) Kobayashi, M.; Harada, M.; Takakura, H.; Ando, K.; Goto, Y.; Tsuneda, T.; Ogawa, M.; Taketsugu, T. Theoretical and Experimental Studies on the Near-Infrared Photoreaction Mechanism of a Silicon Phthalocyanine Photoimmunotherapy Dye: Photoinduced Hydrolysis by Radical Anion Generation. *ChemPlusChem* **2020**, 1−6.
(36) Lumley, E. K.; Dyer, C. E.; Pamme, N.; Boyle, R. W. Comparison of Photo-Oxidation Reactions in Batch and a New Photosensitizer-Immobilized Microfluidic Device. *Org. Lett.* **2012**, *14*, 5724−5727.
(37) Durmuş, M.; Nyokong, T. Synthesis, Photophysical and Photochemical Studies of New Water-Soluble Indium(III) Phthalocyanines. *Photochem. Photobiol. Sci.* **2007**, *6*, 659−668.
(38) Kobayashi, H.; Choyke, P. L. Near-Infrared Photoimmunotherapy of Cancer. *Acc. Chem. Res.* **2019**, *52*, 2332−2339.
(39) Vergara, T. R. C.; Samer, S.; Santos-Oliveira, J. R.; Giron, L. B.; Arif, M. S.; Silva-Freitas, M. L.; Cherman, L. A.; Treitsman, M. S.; Chebabo, A.; Sucupira, M. C. A.; Da-Cruz, A. M.; Diaz, R. S. Thalidomide Is Associated With Increased T Cell Activation and Inflammation in Antiretroviral-Naive HIV-Infected Individuals in a Randomised Clinical Trial of Efficacy and Safety. *EBioMedicine* **2017**, *23*, 59−67.
(40) Samer, S.; Arif, M. S.; Giron, L. B.; Zukurov, J. P. L.; Hunter, J.; Santillo, B. T.; Namiyama, G.; Galinskas, J.; Komninakis, S. V.; Oshiro, T. M.; Sucupira, M. C.; Janini, L. M.; Diaz, R. S. Nicotinamide Activates Latent HIV-1 Ex Vivo in ART Suppressed Individuals, Revealing Higher Potency than the Association of Two Methyltransferase Inhibitors, Chaetocin and BIX01294. *Brazilian J. Infect. Dis.* **2020**, *24*, 150−159.
(41) Chawla, A.; Wang, C.; Patton, C.; Murray, M.; Punekar, Y.; De Ruiter, A.; Steinhart, C. A Review of Long-Term Toxicity of Antiretroviral Treatment Regimens and Implications for an Aging Population. *Infect. Dis. Ther.* **2018**, *7*, 183−195.
(42) Sohl, C. D.; Szymanski, M. R.; Mislak, A. C.; Shumate, C. K.; Amiralaei, S.; Schinazi, R. F.; Anderson, K. S.; Yin, Y. W. Probing the Structural and Molecular Basis of Nucleotide Selectivity by Human Mitochondrial DNA Polymerase γ. *Proc. Natl. Acad. Sci. U. S. A.* **2015**, *112*, 8596−8601.
(43) Timilsina, U.; Gaur, R. Modulation of Apoptosis and Viral Latency—An Axis to Be Well Understood for Successful Cure of Human Immunodeficiency Virus. *J. Gen. Virol.* **2016**, *97*, 813−824.
(44) Kovacs, J. M.; Noeldeke, E.; Ha, H. J.; Peng, H.; Rits-Volloch, S.; Harrison, S. C.; Chen, B. Stable, Uncleaved HIV-1 Envelope Glycoprotein Gp140 Forms a Tightly Folded Trimer with a Native-like Structure. *Proc. Natl. Acad. Sci. U. S. A.* **2014**, *111*, 18542−18547.
(45) Madani, N.; Millette, R.; Platt, E. J.; Marin, M.; Kozak, S. L.; Bloch, D. B.; Kabat, D. Implication of the Lymphocyte-Specific Nuclear Body Protein Sp140 in an Innate Response to Human Immunodeficiency Virus Type 1. *J. Virol.* **2002**, *76*, 11133−11138.
(46) Koyanagi, Y.; Miles, S.; Mitsuyasu, R. T.; Merrill, J. E.; Vinters, H. V.; Chen, I. S. Y. Dual Infection of the Central Nervous System by AIDS Viruses with Distinct Cellular Tropisms. *Science* **1987**, *236*, 819−822.
(47) Pincus, S. H.; Wehrly, K. AZT Demonstrates Anti-HIV-l Activity in Persistently Infected Cell Lines: Implications for Combination Chemotherapy and Immunotherapy. *J. Infect. Dis.* **1990**, *162*, 1233−1238.
(48) Pincus, S. H.; McClure, J. Soluble CD4 Enhances the Efficacy of Immunotoxins Directed against Gp41 of the Human Immunodeficiency Virus. *Proc. Natl. Acad. Sci. U. S. A.* **1993**, *90*, 332−336.
(49) Mchugh, L.; Hu, S.; Lee, B. K.; Santora, K.; Kennedy, P. E.; Berger, E. A.; Pastan, I.; Hamer, D. H. Increased Affinity and Stability of an Anti-HIV-1 Envelope Immunotoxin by Structure-Based Mutagenesis. *J. Biol. Chem.* **2002**, *277*, 34383−34390.
(50) Bahou, C.; Richards, D. A.; Maruani, A.; Love, E. A.; Javaid, F.; Caddick, S.; Baker, J. R.; Chudasama, V. Highly Homogeneous Antibody Modification through Optimisation of the Synthesis and Conjugation of Functionalised Dibromopyridazinediones. *Org. Biomol. Chem.* **2018**, *16*, 1359−1366.
(51) Castañeda, L.; Wright, Z. V. F.; Marculescu, C.; Tran, T. M.; Chudasama, V.; Maruani, A.; Hull, E. A.; Nunes, J. P. M.; Fitzmaurice, R. J.; Smith, M. E. B.; Jones, L. H.; Caddick, S.; Baker, J. R. A Mild Synthesis of N-Functionalised Bromomaleimides, Thiomaleimides and Bromopyridazinediones. *Tetrahedron Lett.* **2013**, *54*, 3493−3495.
(52) Robinson, E.; Nunes, J. P. M.; Vassileva, V.; Maruani, A.; Nogueira, J. C. F.; Smith, M. E. B.; Pedley, R. B.; Caddick, S.; Baker, J. R.; Chudasama, V. Pyridazinediones Deliver Potent, Stable, Targeted and Efficacious Antibody-Drug Conjugates (ADCs) with a Controlled Loading of 4 Drugs per Antibody. *RSC Adv.* **2017**, *7*, 9073−9077.
(53) Mello, B. L.; Alessi, A. M.; Riaño-Pachón, D. M.; DeAzevedo, E. R.; Guimarães, F. E. G.; Espirito Santo, M. C.; McQueen-Mason, S.; Bruce, N. C.; Polikarpov, I. Targeted Metatranscriptomics of Compost-Derived Consortia Reveals a GH11 Exerting an Unusual Exo-1,4-β-Xylanase Activity. *Biotechnol. Biofuels* **2017**, *10*, 1−17.
(54) Marinho, R. D. S. S.; Sanz Duro, R. L.; Santos, G. L.; Hunter, J.; Teles, M. D. A. R.; Brustulin, R.; De Padua Milagres, F. A.; Sabino, E. C.; Diaz, R. S.; Komninakis, S. V. Detection of Coinfection with Chikungunya Virus and Dengue Virus Serotype 2 in Serum Samples of Patients in State of Tocantins, Brazil. *J. Infect. Public Health* **2020**, *13*, 724−729.
(55) Komninakis, S. V.; Santos, D. E. M.; Santos, C.; Oliveros, M. P. R.; Sanabani, S.; Diaz, R. S. HIV-1 Proviral DNA Loads (as Determined by Quantitative PCR) in Patients Subjected to Structured Treatment Interruption after Antiretroviral Therapy Failure. *J. Clin. Microbiol.* **2012**, *50*, 2132−2133.
(56) Kumar, A. M.; Fernandez, J. B.; Singer, E. J.; Commins, D.; Waldrop-Valverde, D.; Ownby, R. L.; Kumar, M. Human Immunodeficiency Virus Type 1 in the Central Nervous System Leads to Decreased Dopamine in Different Regions of Postmortem Human Brains. *J. Neurovirol.* **2009**, *15*, 257−274.
(57) Brenner, S.; Horne, R. A Negative Staining Method For High Resolution Electron Microscopy Of Viruses. *Biochim. Biophys. Acta* **1959**, *34*, 103−110.

https://doi.org/10.1021/acsomega.1c01721
ACS Omega XXXX, XXX, XXX−XXX